smart cities

MDPI

Article

A Comparative Analysis of Multi-Label Deep Learning Classifiers for Real-Time Vehicle Detection to Support Intelligent Transportation Systems

Danesh Shokri [1,2,*], Christian Larouche [1,2] and Saeid Homayouni [3]

[1] Département des Sciences Géomatiques, Université Laval, Québec, QC G1V 0A6, Canada; christian.larouche@scg.ulaval.ca
[2] Centre de Recherche en Données et Intelligence Géospatiales (CRDIG), Université Laval, Québec, QC G1V 0A6, Canada
[3] Centre Eau Terre Environnement, Institut National de la Recherche Scientifique, Québec, QC G1V 0A6, Canada; saeid.homayouni@inrs.ca
* Correspondence: danesh.shokri.1@ulaval.ca

Abstract: An Intelligent Transportation System (ITS) is a vital component of smart cities due to the growing number of vehicles year after year. In the last decade, vehicle detection, as a primary component of ITS, has attracted scientific attention because by knowing vehicle information (i.e., type, size, numbers, location speed, etc.), the ITS parameters can be acquired. This has led to developing and deploying numerous deep learning algorithms for vehicle detection. Single Shot Detector (SSD), Region Convolutional Neural Network (RCNN), and You Only Look Once (YOLO) are three popular deep structures for object detection, including vehicles. This study evaluated these methodologies on nine fully challenging datasets to see their performance in diverse environments. Generally, YOLO versions had the best performance in detecting and localizing vehicles compared to SSD and RCNN. Between YOLO versions (YOLOv8, v7, v6, and v5), YOLOv7 has shown better detection and classification (car, truck, bus) procedures, while slower response in computation time. The YOLO versions have achieved more than 95% accuracy in detection and 90% in Overall Accuracy (OA) for the classification of vehicles, including cars, trucks and buses. The computation time on the CPU processor was between 150 milliseconds (YOLOv8, v6, and v5) and around 800 milliseconds (YOLOv7).

Keywords: Intelligent Transportation System (ITS); road traffic surveillance; vehicle detection and localization; deep neural network structures; highway cameras; smart cities

Citation: Shokri, D.; Larouche, C.; Homayouni, S. A Comparative Analysis of Multi-Label Deep Learning Classifiers for Real-Time Vehicle Detection to Support Intelligent Transportation Systems. *Smart Cities* **2023**, *6*, 2982–3004. https://doi.org/10.3390/smartcities6050134

Academic Editors: Katarzyna Turoń and Andrzej Kubik

Received: 13 September 2023
Revised: 17 October 2023
Accepted: 18 October 2023
Published: 23 October 2023

1. Introduction

Nowadays, having a robust and efficient Intelligent Transportation System (ITS) is a key component of metropolises in relation to (1) dropping consuming fuels, (2) monitoring the emission of carbon dioxide, (3) reducing time wasted behind stop lights, (4) optimizing traffic flow, (5) extending the life of road infrastructures, and noticeably, (6) rationalizing parking space [1,2]. ITS proposes solutions for not only environmental issues like air pollution, but also other issues like time-wasting and costs maintenance when modeling; therefore, urban planners use ITS mainly for environmental concerns, traffic congestion, and economic purposes [3–5]. In addressing environmental concerns, the air quality index will increase if vehicles, especially private cars, spend less time waiting at red lights, as vehicles tend to produce more emissions when stopping. It reduces carbon dioxide emission, as the largest factor in producing greenhouse gas [6]. By counting and tracking vehicles, ITS can predict intersections' density for controlling traffic light systems and easing traffic jams [3,7]. Therefore, an efficient and smooth transportation system is achieved as a result. As estimated by UNICEF, traffic congestion wastes more than USD 100 billion annually, whether by private or state organizations (www.UNICEF.org, accessed on 12 September

2023). Consequently, there are chances of individuals being badly injured in a crash, which will raise problems like individuals' mental and physical health or heavier financial burden.

Recently, the objective of obtaining an efficient ITS is closer to reality due to the advancements in data transmission by fifth Generation (5G) wireless technology [8,9]. This technology transmits information with a speed of between 15 to 20 Gbps (Giga bytes per second), with a latency 10 times better than that of 4G [10]. In addition, advancements in cloud computing systems and Graphic Processing Units (GPUs) attract researchers' attention and enable them to monitor urban dynamics in real time [11]. Therefore, these developments in hardware and data transmission provide an opportunity to enhance ITS structures and implement state-of-art methodologies such as deep learning neural networks for vehicle detection [12]. Vehicle detection is a prominent stage of ITS construction [1,13]. Deep learning algorithms have shown very impressive performances in object detection and classification using a great variety of resources, such as radiometric images [14,15], Light Detection and Ranging (LiDAR) point clouds [16,17], and one-dimensional signals [18]. Face recognition, self-driving vehicles, and language translation are three popular applications of deep learning algorithms [19]. On the other hand, these algorithms are supervised and need huge training datasets to detect objects.

Besides the challenges met by deep learning algorithms, a considerable positive side is vehicle detection, as the most important parameter of ITS [20]. Knowing vehicles' locations can enable us to measure any relevant component of a smart city or traffic (i.e., density, traffic flow, speed). Consequently, various deep learning structures have been proposed for vehicle detection, based on the four popular ITS methodologies of cameras [21], LiDAR point clouds [22], wireless magnetics [23] and radar detectors [13]. In ITS, cameras have shown the most efficient and accurate performance due to their ability to record contextual information, cover a larger area and be affordable, and, notably, they are the only tool that can achieve license plate recognition in illegal situations [2,24]. Most importantly, deep learning structures work on two-dimensional camera images, and do not require any transformation space between image sequences and deep learning layers [25]. This adaptability between camera images and deep learning layers results in the development of numerous algorithms for vehicle detection. Although several morphological procedures, such as opening, have been suggested for vehicle detection, their high sensitivity to illumination changes and weather conditions has made them obsolete [24].

Generally, the deep learning algorithms that have been used most widely in vehicle detection are (i) Single Shot MultiBox Detector (SSD) [26], (ii) Region-Based Convolutional Neural Network (RCNN) [27], and lastly (iii), You Only Look Once (YOLO) [28]. Each of these algorithms has its own benefits and drawbacks in object detection and localization. For example, Faster RCNN, which is a branch of RCNN, shows a better performance in the detection of small-scale objects, while it is not suitable for real-time object detection, unlike SSD and YOLO (www.towardsdatacience.com, accessed on 12 September 2023). Developers have released eight versions of YOLO (e.g., YOLOv1), four versions of RCNN (i.e., RCNN, Mask, Fast, and Faster RCNN) and two SSD versions (i.e., SSD 512 and SSD 300) since 2015 [24,29,30]. For training these methodologies, various free-access benchmark datasets such as COCO, ImageNet Large Scale Visual Recognition Challenge (ILSVRC), and PASCAL VOC, comprising more than 300,000 images, were used. A great variety of objects, ranging from vehicles to animals, have been covered in recognition applications. Since these algorithms have shown their excellent performance in object detection, researchers have used the acquired weights of these deep learning algorithms in other fields, such as the detection of sidewalk cracks [31], fish [31], and weeds [32]. This has been referred to as transfer learning.

Kim, Sung [30] made a comparison between SSD, Faster RCNN, and YOLOv4 in the context of detecting vehicles on road surfaces. Private cars, mini-vans, big vans, mini-trucks, trucks and compact cars were set as the vehicle classes. The weights of deep learning algorithms were adjusted by their training data. They concluded that the SSD had the

fastest performance, at 105 FPS (frame per second), while YOLOv4 reached the highest classification accuracy, at around 98%. In a creative way, Li, Zhang [33] used SSD, RCNN and YOLOv3 for transfer learning in the field of agricultural greenhouse detection. They used high-resolution satellite images provided by Gaofen-2 with a spatial resolution of 2 m. In this case, YOLOv3 achieved the highest performance in terms of both computational time and acquired accuracy. Azimjonov and Özmen [34] suggested that if YOLO can be combined with machine learning classifiers such as Support Vector Machine (SVM), the final effect of YOLO on highway video cameras would increase sharply from about 57% to around 95%.

Similarly, Han, Chang [35] increased YOLO's accuracy by adding low and high features to the YOLO network. The new network was called O-YOLOv2 and was evaluated via application to a KITTI dataset, achieving around 94% accuracy. The studies of [7,36,37] used SSD and RCNN in multi-object recognition, including vehicles.

In summary, previous studies have tried to assess the abovementioned deep learning algorithms in various fields, particularly vehicle recognition, but there are still significant gaps in their application for transportation system purposes. This means that these deep learning structures have rarely been applied to highway cameras in challenging situations such as nighttime. Indeed, this was the main motivation of this study, because vehicles can hardly be seen on nighttime images. Previous works did not consider occlusion situations, wherein parts of vehicles were not recorded by cameras. As occlusion may frequently occur on busy roads, the algorithms should be robust in this context. Also, huge amounts of training data and cloud computing systems were used, which is neither time-efficient nor affordable. We have shown that there is no need to use and collect training data in order to improve the efficiency of the mentioned deep learning algorithms. In addition, illumination changes are a main challenge that has been mostly ignored by previous studies. Since ITS should be robust and usable 24 h a day, the algorithms should show acceptable performance at any time of the day and night. Finally, previous studies have rarely tested their methodologies, including YOLO, SSD and RCNN, on diverse weather conditions such as snowy and rainy days.

This study evaluates the state-of-the-art YOLO, RCNN, and SSD methodologies by application to image sequences captured by highway cameras to detect and classify vehicles. The algorithms must be able to detect any vehicle's state, whether this be shape, color, or even size. Noticeably, video cameras also record information during both night and daytime. Consequently, the key contribution of this study is in making a clear comparison between SSD, RCNN, and YOLO when applied to highway cameras in the following ways:

- Providing the most challenging highway videos. To make an acceptable assessment, they must cover various states of vehicles, such as occlusion, weather conditions (i.e., rainy), low- to high-quality video frames, and different resolutions and illuminations (images collected during the day and at night). Also, the videos must be recorded from diverse viewing angles with cameras installed on top of road infrastructures, in order to determine the best locations. Section 2 covers this first contribution;
- Making a comprehensive comparison between the deep learning algorithms in terms of acquiring accuracy in both vehicle detection and classification. The vehicles are categorized into the three classes of car, truck, and bus. The computation time of the algorithms is also assessed to determine which one presents a better potential usability in real-time situations. Section 3 covers this second contribution.

2. Traffic Video Data

The organization "Ministère des Transports et de la Mobilité durable du Québec", located in the Province of Quebec, Canada, has established numerous online highway cameras. Figure 1 shows nine samples of images acquired with those cameras. The cameras work 24 h a day, covering multiple road lanes under all illumination and weather conditions. Therefore, these cameras are fairly suitable for use in our assessment of the deep learning structures relevant to vehicle detection and localization on highways. The vehicles appear

relatively small on the images, which offer little contextual information due to the distance of the cameras from the road surface and the low resolution of the camera. The dimension of each frame is 352 × 240, and the images were recorded on 14 January 2023.

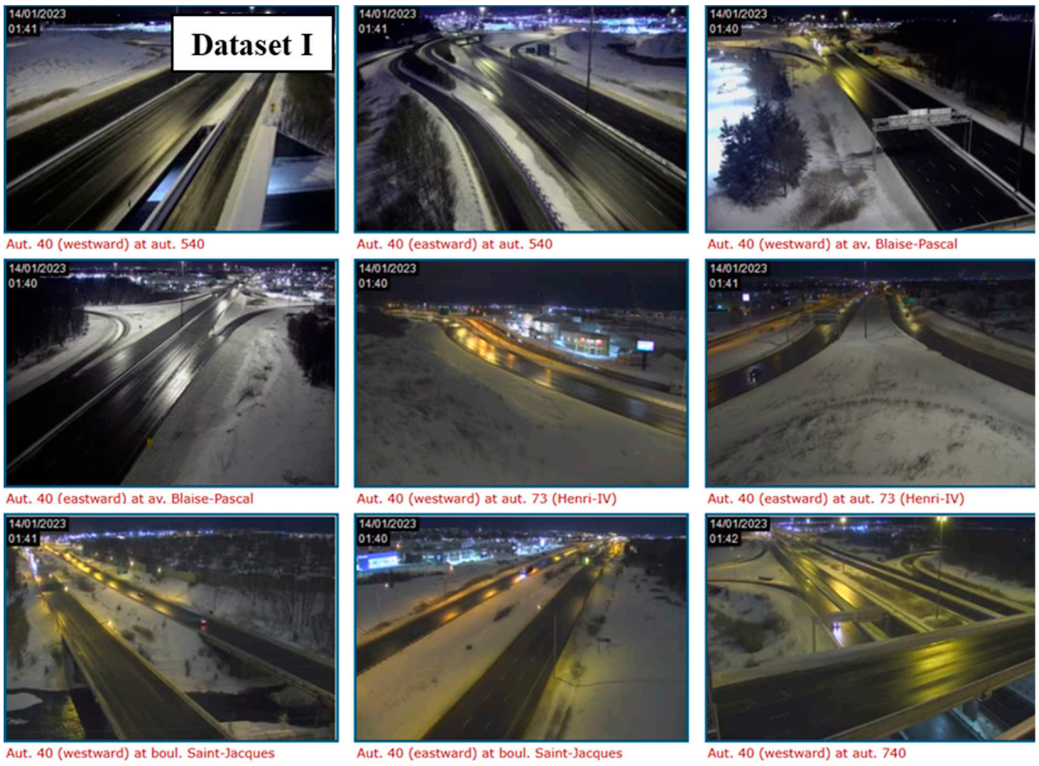

Figure 1. Samples of highway cameras located in Quebec, Canada.

In order to perform a comprehensive assessment of the methodologies, the processed highway videos should cover as many road challenges as possible. Therefore, the next high-quality image datasets were downloaded from YouTube and KAGGLE (www.kaggle.com, accessed on 12 September 2023) platforms (Figure 2). As can be seen in Figure 2, datasets IV and V include numerous vehicles, ranging from cars to buses, shown at night time. The main attribute of these two datasets is that the vehicles' headlights are on, and the vehicles are moving fast in both directions. In other datasets, the cameras are relatively close to the cars on the roads, which results in the collection of more contextual information. Also, the angle of view of some of the cameras (i.e., dataset VII) is not perpendicular to the road infrastructure. This means that vehicles are recorded from a side view, and this increases the complexity of the environments considered. Shawon [38] released a video on KAGGLE, which is an online community platform for data scientists, in order to monitor traffic flow (dataset II). These cameras produce images with a resolution of 1364 × 768 pixels at a frequency of 25 FPS. This high-quality video includes various British vehicles ranging from commercial trucks to private cars. Another positive side of this video is that the vehicles therein move on two separate roads in opposite directions, meaning that the algorithms evaluate front and rear vehicle views. This video also provides more of the contextual information of on-road vehicles, which may enable better vehicle detection and classification. Another British highway dataset was released by Shah [39] including frequent challenging traffic flow types (Dataset III). Table 1 provides a summary of the information of the selected datasets in terms of pixel resolution, time of recording, etc. In the "Section 5.1", we provide precise and in-depth explanations about why these datasets have been chosen.

Figure 2. Views of the selected video datasets used for the evaluation of the deep learning structures.

Table 1. Specification attributes of the selected datasets.

Dataset	Day/Night	Frames	FPS	Height	Width	Rear/Front	Quality	Angle of View (AoV)	Link (accessed on 12 September 2023)
Dataset I	Both	2250	15	352	240	Both	Low	Vertical-Low-High	https://www.quebec511.info/fr/Carte/Default.aspx
Dataset II	Day	1525	25	1364	768	Both	Medium	Low	https://www.kaggle.com/datasets/shawon10/road-traffic-video-monitoring
Dataset III	Day	250	10	320	240	Rear	Low	Vertical	https://www.kaggle.com/datasets/aryashah2k/highway-traffic-videos-dataset

Table 1. *Cont.*

Dataset	Day/Night	Frames	FPS	Height	Width	Rear/Front	Quality	Angle of View (AoV)	Link (accessed on 12 September 2023)
Dataset IV	Night	61,840	30	1280	720	Both	Very High	Vertical	https://www.youtube.com/watch?v=xEtM1I1Afhc
Dataset V	Night	178,125	25	1280	720	Both	Low	Vertical	https://www.youtube.com/watch?v=iA0Tgng9v9U
Dataset VI	Day	62,727	30	854	480	Rear	Medium	Vertical	https://youtu.be/QuUxHIVUoaY
Dataset VII	Day	9180	30	1920	1080	Front	Very High	Low	https://www.youtube.com/watch?v=MNn9qKG2UFI&t=7s
Dataset VIII	Day	107,922	30	1280	720	Front	High	High	https://youtu.be/TW3EH4cnFZo
Dataset IX	Day	1525	25	1280	720	Both	High	Vertical	https://www.youtube.com/watch?v=wqctLW0Hb_0&t=10s

3. Deep Learning Methodologies Applied to Vehicle Detection

The deep neural network structures generally comprise training data, region proposals, feature extraction, layer selection, and classifiers. Figure 3 presents an overview of a deep learning structure used for detecting and identifying a pattern or object in an image.

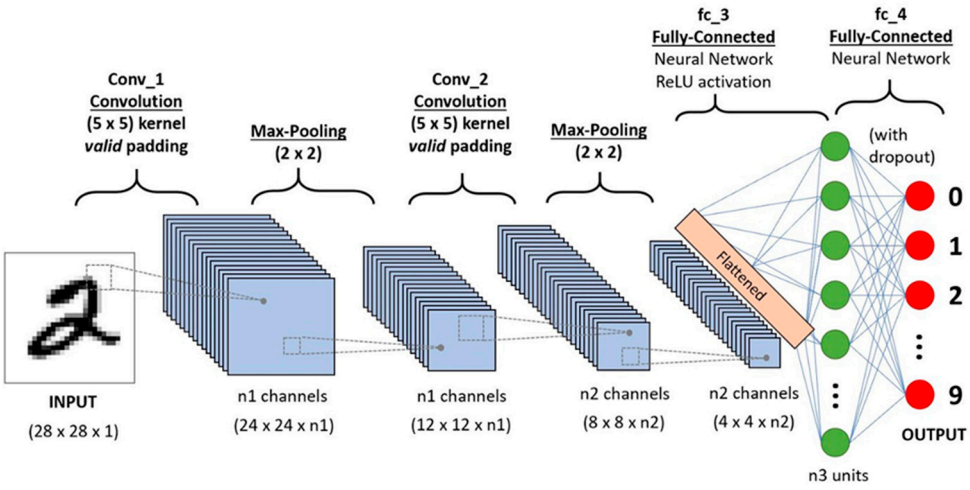

Figure 3. An overview of a deep learning structure [40].

Training Data

Deep learning algorithms are mostly supervised and require pre-defined data, meaning that the images of vehicles, as the research focus of this study, should first be provided to the deep learning network. This process is undertaken by drawing boxes around each known object, such as in Figure 4a. As long as the training data are comprehensive and cover any vehicle state, ranging from color to type, the algorithm will detect vehicles precisely. In relation to this, various inclusive free-access datasets have been released; COCO (Common Objects in Common) and ILSVRC (Large Scale Visual Recognition Challenge) are two samples thereof. These are widely used as benchmark datasets in computer vision. They contain labeled images featuring diverse object categories, object annotations, and segmentation masks for object detection and recognition tasks. Figure 4b shows 400 predefined images from COCO, which include humans, animals, houses, and vehicles. In

order to improve the amount of data and the model's prediction accuracy, augmentation is suggested, which applies varying angular and rotation steps to the original data [41]. This also results in reducing the cost of labeling data, and generates variability and flexibility.

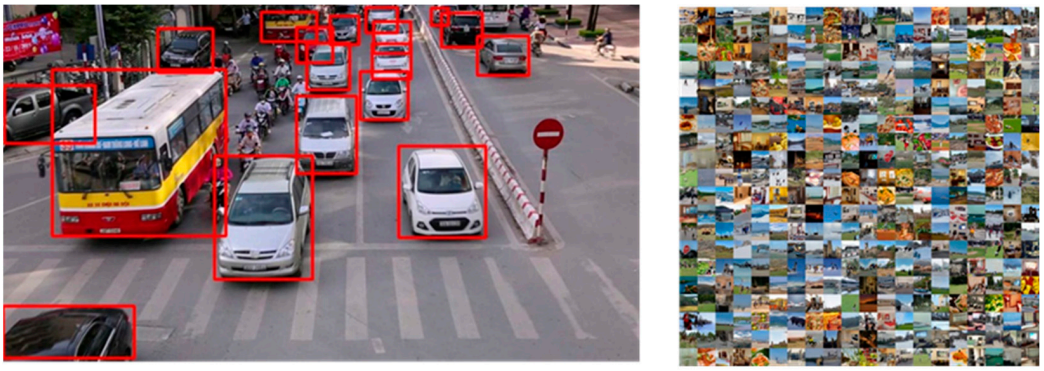

(a) (b)

Figure 4. Training data in order to feed them into deep learning structures [42]; (**a**) bounding boxes around vehicles, (**b**) samples from the COCO dataset used as training data (www.coco.org, accessed on 12 September 2023).

Region Proposals

Traditional algorithms have sought to assess individual pixels from the inputted images for the sake of object detection and localization. This process was shown to be time-consuming due to the required analysis of thousands of pixels by deep layer networks. The state-of-the-art methodologies represent several solutions to finding the candidate pixels, instead of evaluating pixel-by-pixel. For instance, the two SSD and YOLO methods divide the input images into grids of the same length. This process will reduce the computation time sharply as it analyzes only a few cells, instead of thousands of pixels. Assume image I has dimensions of 300×300, and the grid of SSD is 8×8. The computation process will be decreased from approximately 9×10^4 (300×300) to 64.

Feature Extraction

Convolutional layers (*Conv*) represent a popular feature extraction process because they can be used for calculating features without any human supervision. In addition, the convolutional layers prevent overfitting, which is a noticeable problem in machine learning algorithms, as they introduce flexibility in feature learning. A sample of feature extraction model VGG16 is shown in Figure 5a. Via trial and error, researchers have found the optimal convolution size, for example, 3×3 in SSD. Since these layers may feature negative values, an activation function is considered. Various activation functions (Equations (1)–(3)) have been proposed, and ReLU (Equation (1)) is an example thereof. The ReLU converts the negative values of the convolutional layers into zero. To reduce the huge volume of convolution layers, the two steps of max pooling and stride are required, as shown in Figure 5b.

$$\text{ReLU}: \ f(x) = \left\{ \begin{array}{ll} x & x \geq 0 \\ 0 & x < 0 \end{array} \right\} \tag{1}$$

$$\text{Sigmoid}: \ \sigma(x) = \frac{1}{1 + e^{-x}} \tag{2}$$

$$\text{Hyperbolic Tangent}: \ Tanh = \frac{sinhx}{coshx} = \frac{e^x - e^{-x}}{e^x + e^{-x}} \tag{3}$$

where x is the value of the convolution layer's outputs.

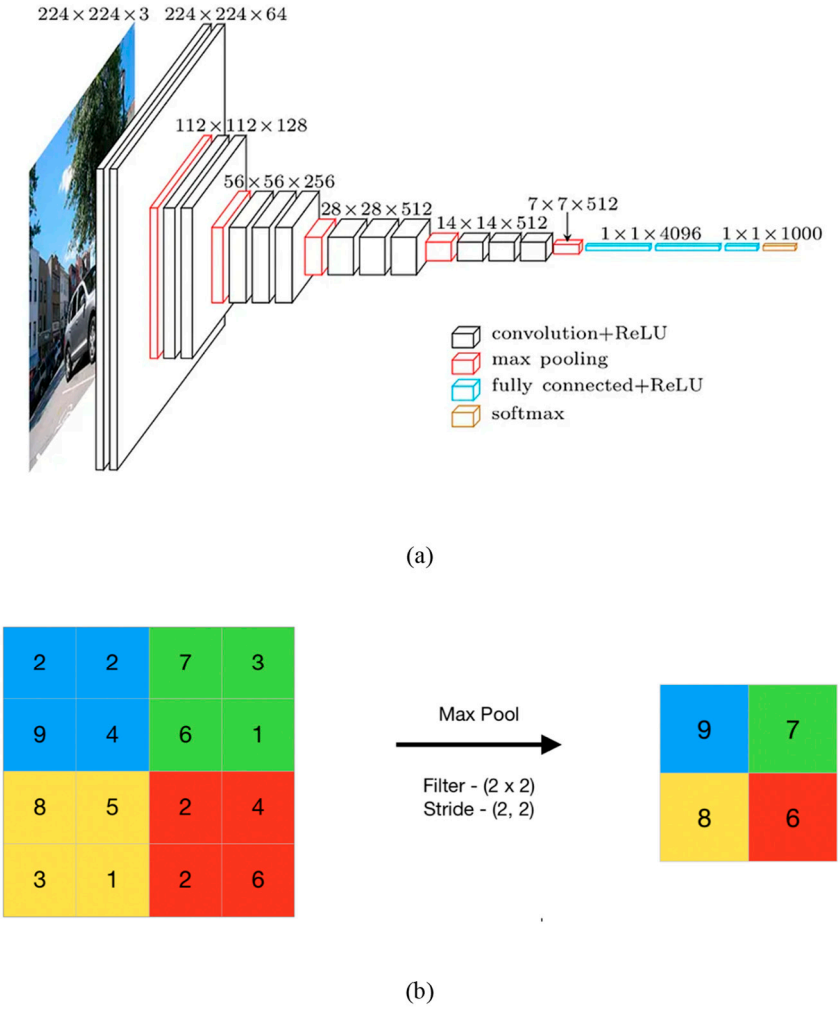

Figure 5. Feature extraction: (**a**) the VGG16 model used for feature extraction (www.towardsdatascience.com, accessed on 12 September 2023); (**b**) applying pooling and stride to a 4 × 4 image (www.geeksforgeeks.org, accessed on 12 September 2023).

Layer Selection and Classifier

After feature extraction and pooling, the remaining features are flattered and fed into the deep-layer neurons. For each neuron, a feature is assigned. Afterward, a full connectivity (*FC*) neural network, which links a neuron to all the neurons in the adjacent layer, is considered. Next, a classifier, which can operate by machine learning, such as a Support Vector Machine (SVM) or a probabilistic model, is required to determine the object type. This classifier assigns a value of $\{0, 1\}$ for each object of interest, whereby the image class has the highest score. To achieve the best performance in object detection and localization, a Back Propagation (BP) step is needed, which measures the weights between neurons and loss functions. The most popular loss functions are maximum likelihood, cross entropy, and Mean Squared Error (MSE) [43]. The loss function determines the difference between the predicted value of an image and its actual class. When the loss function reaches the minimum rate of difference, it is said that the deep learning algorithm works properly; in any other case, the algorithm's structure should be changed and adjusted to ensure higher accuracy.

After setting out how a deep structure works, Figure 6 illustrates the flowcharts of SSD [26], RCNN [44], and YOLO [45] as the most popular vehicle detection methodologies. Each of these procedures features certain stages in the vehicle localization process, described as follows.

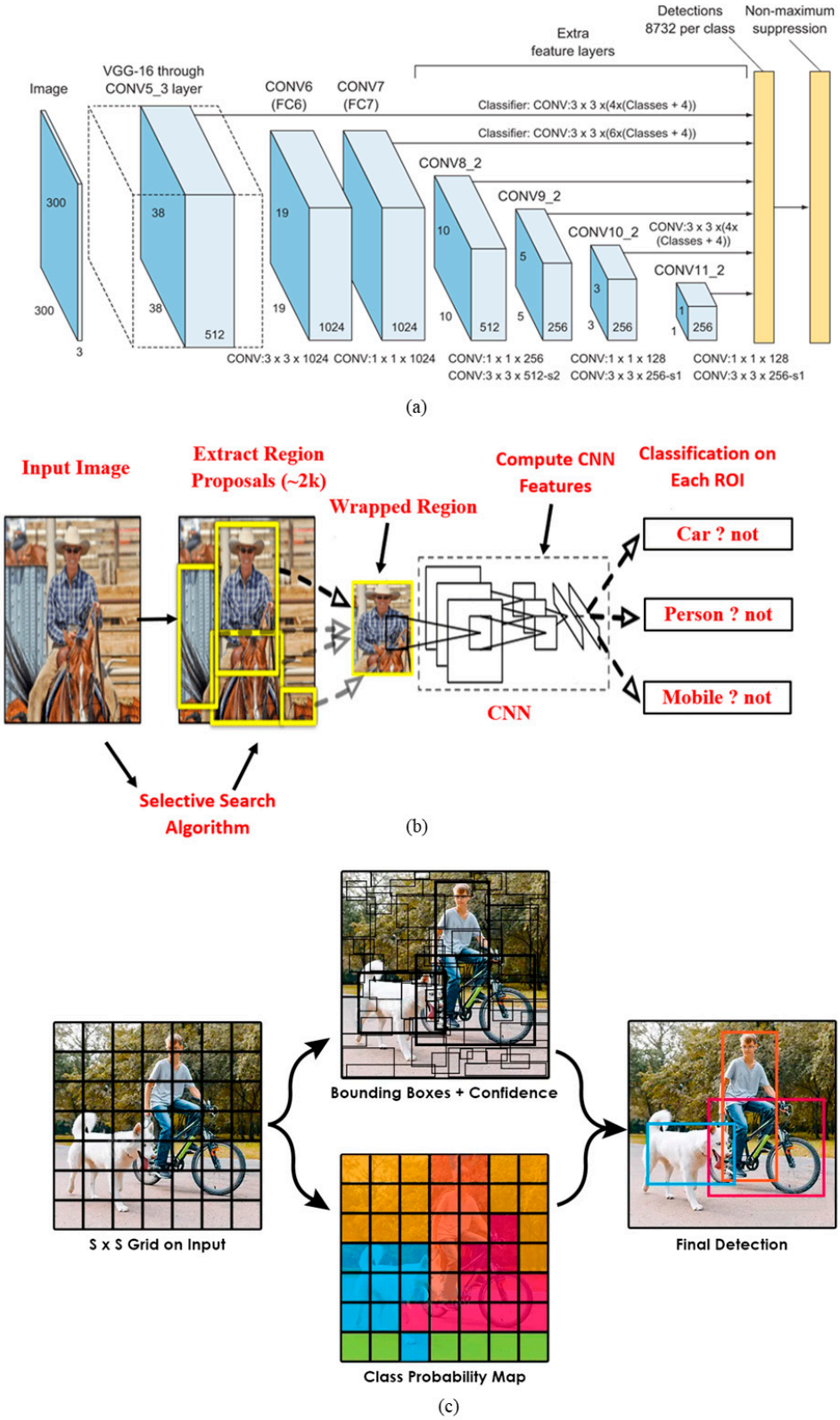

Figure 6. Deep learning structures of (**a**) SSD [26], (**b**) RCNN [44], and (**c**) YOLO [45].

3.1. Single Shot Multi-Box Detector (SSD)

This algorithm was trained and evaluated on the two large free-access datasets Pascal VOC (Pattern Analysis, Statistical Modeling, and Computational Learning—Visual Object Classes) and COCO, and gained an mAP (mean average precision) score of more than 0.74%. SSD initially converts the inputted images, whether they comprise training or test

data, into a feature map (grid) with a size of $m \times n$ (generally, the grid has dimensions of 8×8). Then, multiple boxes of different sizes are placed around each cell. The sizes and directions of these boxes are known. This is why it is called a multibox detector algorithm. Afterwards, features are measured with the help of VGG16 as the base network, due to its exceptional performance in classification and possession of several auxiliary convolutional layers. These features help in measuring multiple boxes' scores between grids, and collecting ground truth data for each SSD class (i.e., vehicle, pedestrians).

The following equations (Equations (4)–(6)) show the process of score calculation for both ground truth boxes (d) and estimated ones (l). Here, l refers to the predicted boxes around each cell. Most corresponding ground truth boxes with l are detected by a matching strategy. The parameter of c is the class (i.e., vehicle, dog, cat, etc.), N is the number of boxes matched with l, and α is considered equal to one by cross-validation. Each box, whether ground truth or estimated, has four parameters of $\{center\ of\ x\ (cx),\ center\ of\ y\ (cy),\ width\ (w)\ and\ height\ (h)\}$.

$$L(x, c, l, g) = \frac{1}{N}\left(L_{conf}(x, c) + \alpha L_{loc}(x, l, g)\right) \tag{4}$$

$$\begin{aligned} L_{loc}(x, l, g) &= \sum_{i \in Pos}^{N} \sum_{m \in \{cx, cy, w, h\}} x_{ij}^{k} smooth_{L1}\left(l_i^m - \hat{g}_j^m\right) \\ \hat{g}_j^{cx} &= \frac{g_j^{cx} - d_i^{cx}}{d_i^w} \qquad \hat{g}_j^{cy} = \frac{g_j^{cy} - d_i^{cy}}{d_i^h} \\ \hat{g}_i^w &= \log\left(\frac{g_j^w}{d_i^w}\right) \qquad \hat{g}_i^h = \log\left(\frac{g_j^h}{d_i^h}\right) \end{aligned} \tag{5}$$

$$L_{conf}(x, c) = -\sum_{i \in Pos}^{N} x_{ij}^{p} \log\left(\hat{c}_i^p\right) \text{ where } \hat{c}_i^p = \frac{\exp\left(c_i^p\right)}{\sum_p \exp\left(c_i^p\right)} \tag{6}$$

3.2. You Only Look Once (YOLO)

Like SSD, YOLO first converts the inputted data into $S \times S$ grids (7×7) of the same length and measure several bounding boxes around each grid cell (two boxes). Then, the five parameters of $cx,\ cy,\ w, h$ and a *confidence score* are measured. The first four parameters represent the bounding box localization, but the *confidence score* refers to the maximum percentage of overlap between the YOLO bounding boxes and the ground truth boxes. This overlap is assessed by the Intersection Over Union (IOU) methodology, and its output is a probability value for each cell. If we consider the number of classes that YOLO can detect to be equal to 20, then $7 \times 7 \times (2 \times 5 + 20) = 1470$ values can be measured for each image. Afterwards, 26 convolutional layers are selected, of which the last two are fully connected. A 1×1 convolutional layer, like GoogleNet, is used for reducing the feature space. Notably, a tiny YOLO has also been released with nine convolutional layers, which is faster than YOLO. The final output of YOLO is a class probability, according to which a value between zero and one is assigned to each class. Therefore, the class with the highest value will be considered the class of the bounding box. As an image may contain no objects, boxes with a *confidence score* of near zero are eliminated, and are not considered in the next stages (this reduces the computation time). YOLO and tiny YOLO have achieved around 63% and 52% mAP accuracy, respectively, on the VOC 2007 dataset, but a 70% mAP accuracy when applied on VOC 2012. The main positive of this method is its ability to extract objects in 45 FPS (Frame Per Second), which means it is suitable for real-time object detection.

To date, eight versions of YOLO have been released for use in object extraction. YOLOv2 includes fine-grained features to improve the accuracy of detecting small objects [46]. Its capacity to detect small and multiscale objects was the main drawback of YOLOv1 [45]. Yolov3 uses logistic classifiers to assign a score to each class, while the previous ones used a SoftMax procedure [47]. YOLOv3 also employs Darknet-53 as the

feature extraction step, with 53 convolutional layers, which is a deep neural network architecture commonly used for object detection and classification tasks. Increasing computation time and detecting object accuracy was the main aim of YOLOv4 [48]. It verified the negative effects of SOTA's Bag-of-Freebies and Bag-of-Specials by use of COCO as the training dataset. YOLOv5 has a lower volume, around 27 MB, in comparison with YOLOv4 (277 MB), both of which were released in 2020 [49]. YOLOv6 showed that if an anchor-free procedure with Varifocal Length (VFL) is used throughout the training steps, the algorithm can run 51% faster than other anchor-based methods [50]. YOLOv7 mainly focused on generating accurate bounding boxes for detecting objects more precisely [51]. Recognizing objects quickly was the foremost goal of YOLOv8, which employed a cutting-edge SOTA model (www.ultralytics.com, accessed on 12 September 2023). This study will evaluate the four last versions of YOLO, i.e., 5, 6, 7, and 8, for use in vehicle detection from highway videos, because these versions are robust in detecting small objects and have optimized computation times.

3.3. Region-Based Convolutional Neural Network (RCNN)

The semantic segmentation (region proposals) of images is the first step of RCNN in the context of decreasing computation time [44]. The four similarities of texture, size, fill, and color are key to initial image segmentation. Afterward, Convolutional Neural Networks (CNN) are applied to each selected segment to extract its features. In this case of feature extraction, pre-trained CNN structures, such as ResNet, VGG19, and EfficientNet, can be used. Finally, multiple SVM procedures are trained to classify the extracted features as a specific object, like a vehicle. Fast-RCNN simultaneously applies a CNN structure to the whole of the inputted image and merges it with the region proposal [52]. This results in the extraction of more features from the region's proposal segments. Faster RCNN uses a region proposal neural network structure instead of similarity conditions [53]. This selective search algorithm, based on neural networks, directly impacts the generation of high-quality region proposals. As the Faster RCNN does not use similarity conditions and is an end-to-end algorithm, the two versions of RCNN and Fast-RCNN are not addressed in this study.

4. Experimental Results

4.1. Accuracy Evaluation

This step provides numerical information on how many vehicles have been correctly detected. The Precision, Recall, and F1 Score accuracies are the most common aspects of algorithm evaluation [54]. The three parameters of True Positive (TP), False Positive (FP), and False Negative (FN) are required to measure accuracy. TP indicates the number of vehicles detected correctly by the algorithms, while FN shows the number of non-vehicles detected falsely as a vehicle. FP specifies the number of vehicles that have not been detected. The Precision accuracy, based on the equations below (Equations (7)–(9)), refers to how many vehicles in the datasets were detected properly, while Recall refers to what percentage of the algorithm's output was vehicles. F1 Score is a performance metric that balances Precision and Recall.

In this stage, TP, FP, and FN are calculated for each individual frame, regardless of whether a vehicle appears in various adjacent frames. Noticeably, as images often include remote areas of a road wherein vehicles are rarely detected, a Region of Interest (RoI) selection stage is needed. The vehicles in dataset II yield acceptable contextual information, but the vehicles located in remote areas of dataset IV, for example, feature less appropriate information. Therefore, ROI is a suitable tool that can be used to assess the real performances of the deep learning algorithms in the context of vehicle detection and classification; thus, the sections of the videos wherein vehicles represent less than 5% of the frame size are not considered in the accuracy calculation because they offer little contextual information. As shown in Table 2, which summarizes the acquired results, YOLOv7 showed the best overall performance on nine datasets in terms of vehicle detection, with around

98% accuracy. The SSD and RCNN have not shown acceptable performances in the context of vehicle detection, with about 58% and less than 2%, respectively.

$$\text{Precision} = \frac{\text{True Positiv}}{\text{True Positive} + \text{False Positive}} = \frac{\text{TP}}{\text{TP} + \text{FP}} \times 100 \quad (7)$$

$$\text{Recall} = \frac{\text{True Positiv}}{\text{True Positive} + \text{False Negative}} = \frac{\text{TP}}{\text{TP} + \text{FN}} \times 100 \quad (8)$$

$$\text{F1} - \text{score} = 2 \times \frac{\text{Precision} \times \text{Recall}}{\text{Precision} + \text{Recall}} \times 100 \quad (9)$$

Table 2. Results acquired by the deep learning structures applied to nine datasets.

		Yolov8	**Yolov7**	**Yolov6**	**Yolov5**	**Faster RCNN**	**SSD**
Dataset I	Precision	43.03	96.33	48.96	54.98	2.00<	2.00<
	Recall	55.41	100.00	78.39	65.40	2.00<	2.00<
	F1-score	48.44	98.13	60.27	59.74	2.00<	2.00<
Dataset II	Precision	99.38	100.00	100.00	100.00	92.49	2.00<
	Recall	100.00	100.00	96.78	99.11	100.00	2.00<
	F1-score	99.69	100.00	98.36	99.55	96.10	2.00<
Dataset III	Precision	87.84	97.36	98.25	96.74	2.00<	2.00<
	Recall	83.56	100.00	99.69	100.00	2.00<	2.00<
	F1-score	85.65	98.66	98.96	98.34	2.00<	2.00<
Dataset IV	Precision	98.42	100.00	100.00	100.00	37.24	2.00<
	Recall	99.68	99.47	96.54	96.55	98.44	2.00<
	F1-score	99.05	99.73	98.24	98.24	54.04	2.00<
Dataset V	Precision	96.33	97.77	95.87	94.38	2.00<	2.00<
	Recall	97.96	98.69	93.14	96.73	2.00<	2.00<
	F1-score	97.14	98.23	94.49	95.54	2.00<	2.00<
Dataset VI	Precision	100.00	100.00	99.18	100.00	88.92	2.00<
	Recall	96.57	99.98	100.00	99.23	100.00	2.00<
	F1-score	98.26	99.99	99.59	99.61	94.14	2.00<
Dataset VII	Precision	99.82	99.85	98.67	100.00	97.57	2.00<
	Recall	78.36	86.14	80.22	85.64	98.61	2.00<
	F1-score	87.80	92.49	88.49	92.26	98.09	2.00<
Dataset VIII	Precision	96.28	99.43	97.65	99.44	96.73	2.00<
	Recall	56.47	100.00	80.25	97.82	99.37	2.00<
	F1-score	71.19	99.71	88.10	98.62	98.03	2.00<
Dataset IX	Precision	100.00	98.23	98.00	99.11	73.29	2.00<
	Recall	93.66	98.37	84.36	99.86	85.37	2.00<
	F1-score	96.73	98.30	91.52	99.48	78.87	2.00<
Average	Precision	91.23	98.77	92.95	93.85	54.69	2.00<
	Recall	84.63	98.07	89.93	93.37	65.31	2.00<
	F1-score	87.10	98.42	91.42	93.61	58.36	2.00<

4.2. Localization Accuracy

The localization accuracy refers to how precisely the algorithms can estimate the positions of vehicles. The Root Mean Square Error (RMSE), as the most common method used in position evaluation, shows the amount of difference between the bounding box predicted with parameters of $\{P_{cx}, P_{cy}, P_w, P_h\}$ and the ground truth bounding box $\{G_{cx}, G_{cy}, G_w, G_h\}$. As the ground truth datasets were unavailable, the bounding boxes around vehicles were drawn by an expert. The library of labels in the Python environment [55], a useful application for bounding box-drawing (called labeling), has been used because it is fast and

user-friendly. In total, 200 vehicles were randomly selected, and we observed that the YOLO versions achieved the best performance when used for localization estimation, with RMSE values lower than 30 pixels. This value was more than 500 pixels for Faster RCNN. Between the YOLO versions, YOLOv8 showed a weaker performance in localization estimation. In the "Section 5.3", we clearly compare the acquired and estimated localization accuracies between the methods.

$$RMSE_i = \sum_{i=1}^{n} \sqrt{(G_{cx} - P_{cx})^2{}_i + (G_{cy} - P_{cy})^2{}_i + (G_w - P_w)^2{}_i + (G_h - P_h)^2{}_i} \quad (10)$$

where n is the number of bounding boxes considered in calculating the different localization accuracies between the estimations of the deep learning algorithms (P) and the ground truth (G). G_{cx} and G_{cy} are, respectively, the centers of the bounding box on the x-axis and y-axis, and G_w, and G_h are the width and height of the ground truth bounding boxes (G). This is also true for the bounding boxes estimated by the algorithms. P_{cx} and P_{cy} are, respectively, the centers of the bounding boxes on the x-axis and y-axis, and P_w and P_h are the width and height of the estimated bounding boxes (G).

4.3. Running Time

In terms of computational time, it is necessary to run the deep learning codes in similar environments to assess which algorithm achieves faster in vehicle detection. Here, we used a personal laptop computer system with the following specifications: Windows 10, RAM 16 G DDR3, Processors of Intel (R) Core (TM) i7-4700 HQ CPU @ 2.4 GHz. Python was used as the programming environment. During the processing of the deep learning code, other non-relevant apps, such as web browsers, that required RAM or CPU resources were turned off to avoid a slowdown of the processing time. Only the CPU was considered in the analysis of the processing time. Other processors, the RAM, and the Graphics Processing Unit (GPU) were neglected. It is worth mentioning that using GPU can sharply reduce the computation time and render the algorithms suitable for the real-time monitoring of roadway infrastructures. Assuming a camera records 30 frames per second (FPS = 30), an algorithm can be used in real-time monitoring if it extracts vehicles at less than 1/30 s = 0.033 s or 33 milliseconds (ms) from each frame. Figure 7 shows the computation times of YOLO versions and Faster RCNN on 1000 frames. As can be seen, YOLOv5 and YOLOv8 achieved the best performance, at around 100 ms, while Faster RCNN took about 2.5 s per frame. YOLOv7, which showed the best overall performance out of the nine datasets in vehicle detection, required around 800 ms per frame.

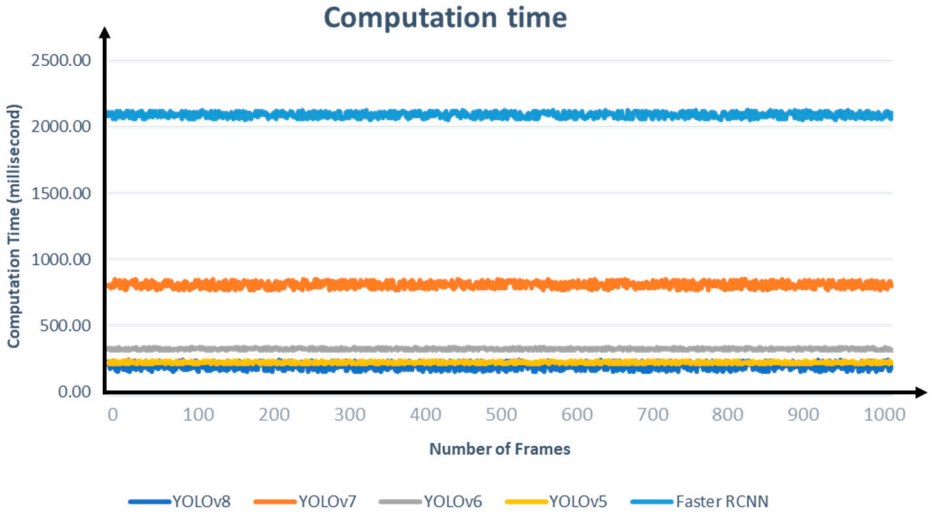

Figure 7. The computation times of YOLO versions and Faster RCNN over 1000 frames.

4.4. Vehicle Classification

The capacity to determine the class of each detected vehicle (i.e., private car, truck, bus) is a strength of the deep learning structures. This is because of the availability of free-access datasets such as COCO [56], which provide not only localization information using bounding boxes, but also the types of each of the objects. Section 4.1 shows how the deep learning algorithms work frame by frame, regardless of whether a vehicle appears in multiple consecutive frames [57].

In order to evaluate errors in the classification procedure, a confusion matrix is used. The parameters of the proposed confusion matrix can be seen in Table 3. This matrix has two axes corresponding to an object's actual and predicted values. For example, the column of the car has three parameters of $\{P_{CC},\ P_{TC},\ P_{BC}\}$, the sum of which equals the real number of vehicles in the region. But the row of cars $\{P_{CC},\ P_{CT},\ P_{CB}\}$ displays how many objects were detected as cars by the algorithms. The diagonal cells of $\{P_{CC},\ P_{TT},\ P_{BB}\}$ that have been highlighted in green are true positive values, representing correctly classified vehicles. The non-diagonal cells highlighted in orange are falsely classified vehicles. The following three parameters, Commission Error (CE), Overall Accuracy (OA), and Omission Error (OE), estimate the accuracy of the classification. Equations (11)–(17) show how the OA, CE, and OE parameters are measured to complete the confusion matrix. This algorithm performs best when the OA is near 100%, and the CE and OE are close to 0%. Table 4 displays the confusion matrix evaluated for each dataset, wherein the OA of each region is highlighted in grey. Similar to the vehicle detection results obtained in Section 4.1, the YOLOv7 algorithm again showed the best performance in object classification. In the Section 5.3, the acquired confusion matrixes are assessed in greater depth in order to better understand the algorithm's performance.

$$\text{Overall Accuracy} = \frac{P_{CC} + P_{TT} + P_{BB}}{P_{CC} + P_{CT} + P_{CB} + P_{TC} + P_{TT} + P_{TB} + P_{BC} + P_{BT} + P_{BB}} \times 100 \quad (11)$$

$$CE_C = \frac{P_{CT} + P_{CB}}{P_{CC} + P_{CT} + P_{CB}} \times 100 \quad (12)$$

$$CE_T = \frac{P_{TC} + P_{TB}}{P_{TC} + P_{TT} + P_{TB}} \times 100 \quad (13)$$

$$CE_B = \frac{P_{BC} + P_{BT}}{P_{BC} + P_{BT} + P_{BB}} \times 100 \quad (14)$$

$$OE_C = \frac{P_{TC} + P_{BC}}{P_{CC} + P_{TC} + P_{BC}} \times 100 \quad (15)$$

$$OE_T = \frac{P_{CT} + P_{BT}}{P_{CT} + P_{TT} + P_{BT}} \times 100 \quad (16)$$

$$OE_B = \frac{P_{CB} + P_{TB}}{P_{CB} + P_{TB} + P_{BB}} \times 100 \quad (17)$$

Table 3. Parameters of a confusion matrix used for classification accuracy evaluation.

		Actual			
		Car	**Truck**	**Bus**	**Commission Error**
Predicted	Car	P_{CC}	P_{CT}	P_{CB}	CE_C
	Truck	P_{TC}	P_{TT}	P_{TB}	CE_T
	Bus	P_{BC}	P_{BT}	P_{BB}	CE_B
	Omission Error	OE_C	OE_T	OE_B	Overall Accuracy

Table 4. Confusion matrix of YOLO versions used for the evaluation of vehicle classification. A grey color is used to highlight the OA.

		Yolov8				**Yolov7**				**Yolov6**				**Yolov5**			
		Car	Truck	Bus		Car	Truck	Bus		Car	Truck	Bus		Car	Truck	Bus	
Dataset I	Car	115	12	0	9.45	255	3	0	1.16	131	6	0	4.38	144	6	0	4.00
	Truck	3	14	0	17.65	7	29	0	19.44	3	22	0	12.00	12	17	0	41.38
	Bus	0	0	0	N/A	0	0	0	N/A	0	0	0	N/A	0	3	0	N/A
		2.54	46.15	N/A	88.97	2.67	9.38	N/A	96.60	2.24	21.43	N/A	94.44	7.69	34.62	N/A	89.94
Dataset II	Car	63	0	0	0.00	63	0	0	0.00	62	3	0	4.62	60	0	0	0.00
	Truck	0	10	0	0.00	0	11	0	0.00	1	8	0	11.11	3	11	0	21.43
	Bus	0	1	0	N/A	0	0	0	N/A	0	0	0	N/A	0	0	0	N/A
d		0.00	9.09	N/A	98.65	0.00	0.00	N/A	100.00	1.59	27.27	N/A	94.59	4.76	0.00	N/A	95.95
Dataset III	Car	50	4	0	7.41	59	1	0	1.67	51	4	0	7.27	49	6	0	10.91
	Truck	2	10	0	16.67	2	11	0	15.38	3	11	0	21.43	1	12	0	7.69
	Bus	2	3	0	N/A	0	0	0	N/A	0	1	0	N/A	3	4	0	N/A
		7.41	41.18	N/A	84.51	3.28	8.33	N/A	95.89	5.56	26.67	N/A	88.57	7.55	45.45	N/A	81.33
Dataset IV	Car	1405	66	17	5.58	1402	55	7	4.23	1410	62	14	5.11	1408	60	6	4.48
	Truck	9	264	16	8.65	12	284	11	7.49	6	276	15	7.07	8	272	18	8.72
	Bus	0	18	27	40.00	0	9	42	17.65	0	10	31	24.39	0	16	36	30.77
		0.64	23.26	55.00	93.08	0.85	18.39	30.00	94.84	0.42	20.69	48.33	94.13	0.56	21.84	40.00	94.08
Dataset V	Car	2758	2	1	0.11	2758	2	0	0.07	2758	3	0	0.11	1750	2	0	0.11
	Truck	0	6	1	14.29	0	6	1	14.29	0	5	2	28.57	6	6	1	14.29
	Bus	0	0	3	0.00	0	0	4	0.00	0	0	3	0.00	0	0	4	0.00
		0.00	25.00	40.00	99.86	0.00	20.00	20.00	99.89	0.00	37.50	40.00	99.82	0.34	25.00	20.00	99.49
Dataset VI	Car	494	13	0	2.56	503	11	0	2.14	496	13	0	2.55	481	16	0	3.22
	Truck	44	72	0	37.93	35	76	0	31.53	39	69	0	36.11	57	71	0	44.53
	Bus	0	9	5	64.29	0	7	5	58.33	0	10	5	66.67	0	7	5	58.33
		8.18	23.40	0.00	89.64	6.51	19.15	0.00	91.68	7.29	25.00	0.00	90.19	10.59	24.47	0.00	87.44
Dataset VII	Car	183	13	0	6.63	282	3	0	1.05	237	6	0	2.47	245	6	0	2.39
	Truck	17	29	0	36.96	5	61	0	7.58	11	50	0	18.03	13	48	0	21.31
	Bus	87	23	4	3.51	0	1	4	20.00	39	9	4	7.69	29	11	4	90.91
		36.24	55.38	0.00	60.67	1.74	4.69	0.00	97.47	17.42	23.08	0.00	91.80	14.63	26.15	0.00	90.83
Dataset VIII	Car	438	20	0	4.37	438	0	0	0.00	438	0	0	0.00	438	0	0	0.00
	Truck	0	58	0	0.00	0	268	0	0.00	0	263	0	0.00	0	266	0	0.00
	Bus	0	214	0	N/A	0	0	0	N/A	0	5	0	N/A	0	2	0	N/A
		0.00	79.86	N/A	67.95	0.00	0.00	N/A	100.00	0.00	1.87	N/A	99.29	0.00	0.75	N/A	99.72
Dataset IX	Car	149	2	0	1.32	152	0	0	0.00	151	7	0	4.43	150	8	0	5.06
	Truck	3	14	0	17.65	0	19	0	0.00	1	12	0	7.69	2	9	0	18.18
	Bus	0	3	0	N/A	0	0	0	N/A	0	0	0	N/A	0	2	0	N/A
		1.97	26.32	N/A	95.32	0.00	0.00	N/A	100.00	0.66	36.84	N/A	95.32	1.32	52.63	N/A	92.98

5. Discussion

5.1. Datasets Challenges and Advantages

This section addresses the challenges the selected video datasets met in covering an important portion of the possible scenarios that could arise in traffic flow monitoring. These various and representative datasets can be used to evaluate cutting-edge deep learning vehicle detection algorithms more completely. First, illumination changes and shadow, as the most important challenge met by radiometric cameras due to their sensitivity to brightness, appear in datasets IV and V (Figure 8a,b). Secondly, a large variety of vehicles, ranging from private cars with diverse sizes and colors to large heavy vehicles such as

buses, can be found in dataset VIII (Figure 8c) and dataset IV (Figure 8a). These vehicles can be found in several countries, such as Canada and England. Notably, a range of fields of view, set by different relations between the cameras and road surfaces (i.e., vertical, low oblique, high oblique), were considered as they provide different types of contextual information. For example, more vehicle bodies can be recorded by high oblique cameras (dataset VIII), while the top parts of vehicles can only be recorded by cameras with a vertical view (dataset VII) (Figure 8c,d).

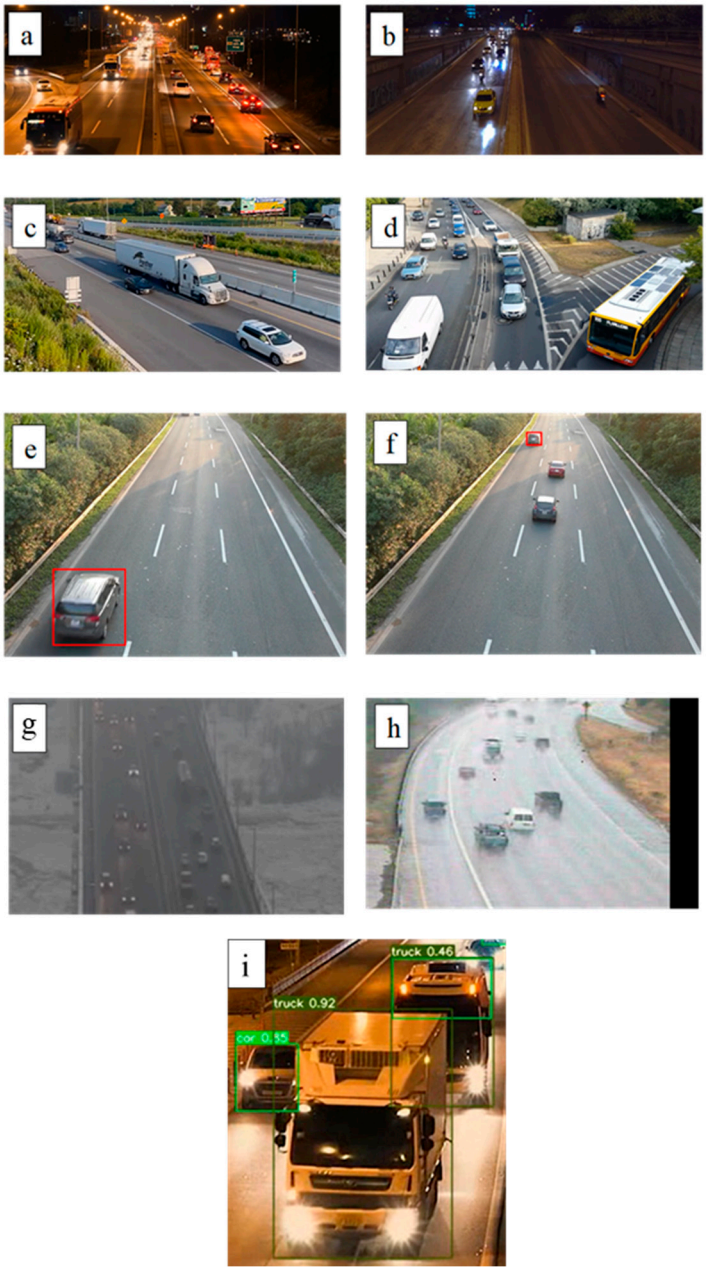

Figure 8. Datasets' challenges; (**a**,**b**) illumination and shadow; (**c**,**d**) high oblique and low oblique angles of view; (**e**,**f**) scale variation of vehicles; (**g**,**h**) weather conditions such as foggy and rainy; (**i**) detection of vehicles that were occluded.

Furthermore, the variation in scale of each individual vehicle is another challenge for the algorithms, which must be robust in this situation (Figure 8e,f). This variation is caused by the perspectives of cameras, meaning that an object near the camera will show a larger scale than more distant objects. The selected datasets also cover different weather

conditions such as rainy and foggy to assess whether the algorithms can still detect vehicles (Figure 8g,h). Finally, vehicle occlusion, shown in Figure 8i, is another parameter that was covered by the datasets. The YOLOv7 algorithm seemed to work properly in such situations of unclear or inaccurate information.

5.2. Parameters Sensitivity

This section discusses various models of each YOLO version in terms of their computation time and acquired classification accuracy. The authors of the YOLO structures, unlike SSD or RCNN, released the five models of $\{n, s, m, l, x\}$, which have been sorted based on obtained accuracy and volume of parameters [28]. These models are generated via trial-and-error. Table 5 displays the model given by YOLOv8, with input values of image size—640 $\times$ 640, mean average precision (mAP), and parameter volume (million). The parameter volume includes network architecture, activation functions, learning rate, batch size, regularization techniques, and optimization algorithms. As can be seen, the YOLOv8n showed a faster performance on the COCO dataset, while the lowest accuracy in object classification. Although the model of YOLOv8x showed the greatest computation time and the best classification accuracy, we also tested this model on our dataset. We observed that it failed to improve vehicle detection accuracy in comparison to YOLOv8n, but also has the potential to extract false objects (Figure 9a). Since the real-time monitoring of vehicles is the main purpose of ITS, the model of {n} has been used across all YOLO versions. Figure 9b compares the YOLO versions, and we can see that YOLOv8 exhibited superior performance in COCO classification. However, our study demonstrates that YOLOv8 had a lower classification accuracy than YOLOv7 when applied to the highway datasets. To gain a deeper understanding of the parameters mentioned in Table 5 and the methods of calculating them, it is recommended to refer to the paper [58] for further insights.

Model of YOLOv8n *Model of YOLOv8x*

(a)

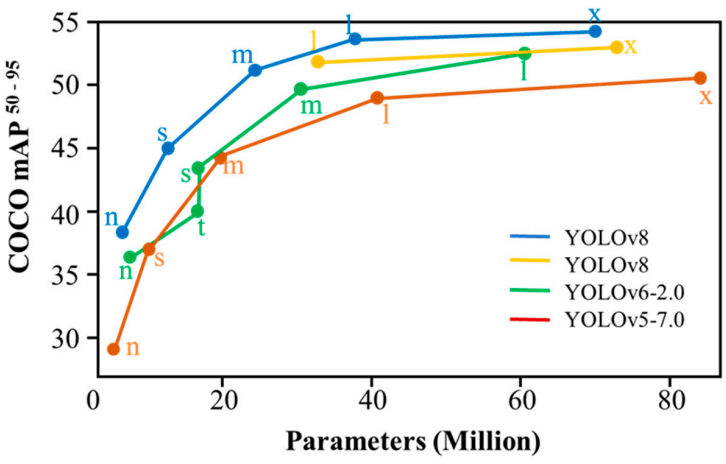

(b)

Figure 9. Parameter sensitivity of YOLO models: (**a**) outputs of two models of YOLO8; (**b**) comparison of YOLO models in terms of parameters' volume and acquired accuracies.

Table 5. Summary of YOLOv8 models.

Model	Size (Pixels)	mAP^{val}	Speed CPU ONNX	Speed A100 Tensor RT	Params (M)	FLOPs
YOLOv8n	640	37.3	80.4	0.99	3.2	8.7
YOLOv8s	640	44.9	128.4	1.20	11.2	28.6
YOLOv8m	640	50.2	234.7	1.83	25.9	78.9
YOLOv8l	640	52.9	375.2	2.39	43.7	165.2
YOLOv8x	640	53.9	479.1	3.53	68.2	257.8

5.3. Algorithms Comparison

This stage gives comparative information about the algorithms regarding vehicle detection, computation time, localization, and classification. Table 4 displays the accuracy acquired by the algorithms when applied to the nine selected datasets. As can be seen, YOLOv7 achieved the best vehicle detection accuracy, with a performance of 98.77%, while Faster RCNN and SSD showed the weakest performance, at about 50%. Also, the localization accuracy of Faster RCNN (Figure 10) and its computation time (Figure 7) were lower than those of the YOLO versions. According to our experimentation, Faster RCNN and SSD algorithms are unsuitable for use in highway vehicle detection. Except for dataset I, where YOLOv7 clearly showed the best detection performance, all YOLO versions have shown an acceptable vehicle detection performance above 90%. This means all YOLO versions work properly in day and nighttime, such as shown in dataset IV, reaching an accuracy above 98%. Also, all YOLO algorithms, especially YOLOv7, work properly in the diverse weather conditions presented in datasets I and III, with an accuracy of around 90%. In addition, our series of tests have demonstrated that the camera resolutions, angle of view (vertical, oblique, high oblique), diversity of vehicles, and even vehicle rear/front view have not negatively impacted the YOLO results. It is logical to conclude that the version YOLOv7 is the best vehicle detection and localization model. The recall accuracy of YOLOv7 was also the highest compared to the other models, while it was slower in terms of computation time.

One noteworthy observation is the remarkable performance of all YOLO versions, especially YOLOv7, when applied to nighttime datasets (dataset IV and dataset V). The results underscore YOLOv7's exceptional capacity for accurately detecting vehicles during low light conditions, with an impressive accuracy exceeding 99%. Following closely, YOLOv8 also demonstrated a commendable performance, achieving an accuracy rate of approximately 98%. This outcome showcases the robustness and adaptability of these YOLO versions, shedding light on their potential applications in scenarios wherein darkness challenges visibility. These findings validate the efficacy of these models, and emphasize their relevance to real-world applications wherein nighttime surveillance and object detection are essential.

Following vehicle detection, a critical parameter for algorithm evaluation is the accuracy of classifying vehicles into car, truck, and bus categories. In this case, the OA (Equation (11)) parameter in Table 4 again shows that YOLOv7 was the best classifier, achieving a value of 97.37%, followed by YOLOv6 at 94.24%. Furthermore, the sums of errors of CE (Equations (12)–(14)) and OE (Equations (15)–(17)) were obtained per class in Table 4. As can be seen, private cars were more accurately detected, with the lowest errors of around 10%, while trucks and buses represented the greatest challenge in classification. The confusion matrix of dataset VIII presented in Table 4 shows the lowest rates of OE and CE errors. This is because oblique-view cameras capture more contextual information, which aids the algorithms in achieving superior classification.

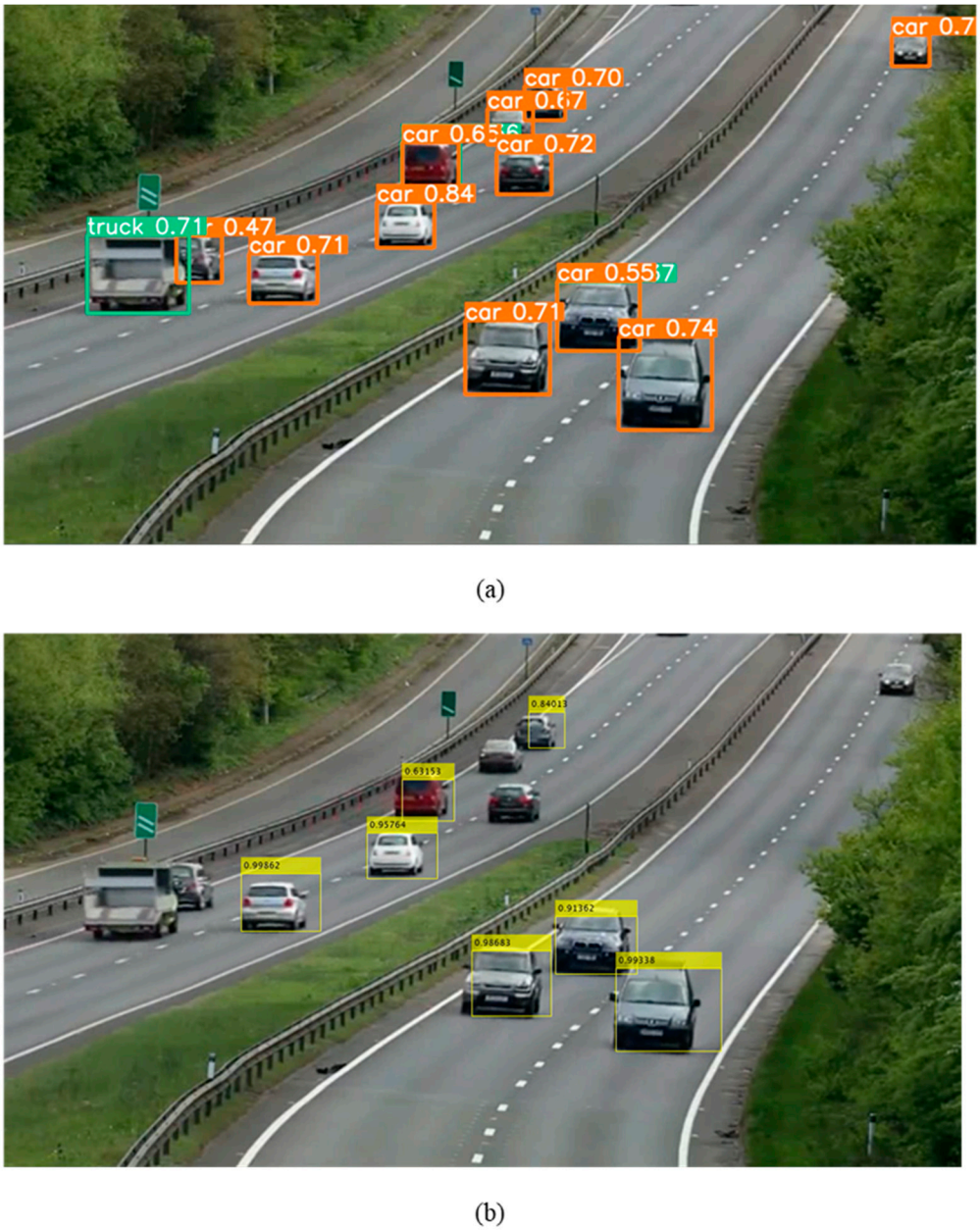

Figure 10. Localization accuracy of (**a**) YOLO and (**b**) Faster RCNN algorithms.

5.4. Comparison with Previous Studies

We here introduce a novel method for comparing state-of-the-art vehicle detection algorithms. This comparison process makes us of challenging highway video datasets with various angles of view. These challenging datasets have not been addressed in previous studies, such as the one by Kim and Sung [30], which conducted a similar comparison between RCNN, SSD, and YOLO. They did not evaluate the algorithms in different illumination contexts, such as nighttime, and different weather conditions. Also, they customized the weights of each algorithm on their training data, which is time-consuming. Indeed, needing no additional training data is one benefit of our work. We suggest that future researchers use the primary model of each released algorithm for vehicle detection, without using any training data. Likewise, Song and Liang [59] used thousands of training data in customizing the weights of YOLO.

Similarly, Zhang, Hu [37] tried to enhance the performance of SSD for vehicle detection at night. Despite improving the SSD algorithm and achieving better detection and classification accuracy, its acquired accuracies (around 89%) are still lower than those of the

YOLO versions (at about 98%). Neupane and Horanont [60] used the models produced by the YOLO versions as the base for transfer learning when enhancing training data, similarly to the previous works. In this case, they did not consider various cameras with different resolutions, or even illumination changes. Also, the enhanced YOLOs were not assessed in both night and daytime. A couple of studies on vehicle-board cameras have been published in the context of the evaluation of deep learning in vehicle detection [35,36]. Since these cameras have a completely different structures and fields of view from highway ones, this is not an effective way to compare the algorithms.

In conclusion, there is no need for additional training data to enhance the performance of YOLO versions in vehicle detection. The released versions of YOLO work effectively in vehicle detection and classification, without any considerable errors in localization. Heavy trucks are detected more accurately when the camera's angle of view is oblique, while private cars are detectable with precision from any direction of view. Noticeably, the algorithm can be run in real-time situations if a GPU processor is used.

6. Conclusions and Future Works

In this paper, we have compared state-of-the-art deep learning algorithms, such as SSD, RCNN, and different versions of YOLO, for vehicle detection. These deep learning structures have been trained and tested on thousands of images acquired from highway cameras and contained in the COCO library. Nine video cameras facing potential challenges were selected for a fair and general comparison, covering a large spectrum of vehicle positions and shapes. These challenging datasets cover numerous angles of view between the camera and road, with different qualities of video (from both day and night) and variations in the scale of vehicles. The YOLO versions, particularly YOLOv7, achieved the best detection and localization accuracy, and the most accurate vehicle classification results for cars, trucks, and buses. In addition, the computation time of the YOLOs was under one-tenth of a second when using a CPU processor. This means the running time will be near real-time if GPU and RAM are used in addition to a CPU processor. With an accuracy in vehicle detection of about 98%, the YOLO versions can generally be used for ITS purposes such as real-time traffic flow monitoring.

In future research, it is strongly recommended to further evaluate deep learning architectures by application to Unmanned Aerial Vehicle (UAV) videos, which can encompass larger road areas. This will address the significant lack of accuracy in the classification of heavy vehicles, such as buses, which should be a priority. Furthermore, investigating the potential for the accurate localization and tracking of detected vehicles is crucial. These enhancements are anticipated to yield more realistic data for road traffic simulators.

Author Contributions: Conceptualization, D.S. and C.L.; methodology, D.S., C.L. and S.H.; software, D.S, C.L. and S.H.; validation, C.L. and S.H.; formal analysis, C.L. and S.H.; investigation, D.S.; resources, D.S.; data curation, D.S.; writing—original draft preparation, D.S.; writing—review and editing, C.L. and S.H.; visualization, D.S.; supervision, C.L. and S.H.; project administration, C.L.; funding acquisition, C.L. and S.H. All authors have read and agreed to the published version of the manuscript.

Funding: This research was funded by Mitacs grant number IT30935 and Semaphor.ai.

Data Availability Statement: Data sharing is not applicable to this paper.

Acknowledgments: The authors would like to thank all the individuals and organizations who made these datasets and algorithms available. In particular, we want to express our sincere appreciation and gratitude to the Semaphor.ai team and Mitacs for their funding support in making this project possible.

Conflicts of Interest: The authors declare no conflict of interest.

References

1. Lv, Z.; Shang, W. Impacts of intelligent transportation systems on energy conservation and emission reduction of transport systems: A comprehensive review. *Green Technol. Sustain.* **2023**, *1*, 100002. [CrossRef]
2. Pompigna, A.; Mauro, R. Smart roads: A state of the art of highways innovations in the Smart Age. *Eng. Sci. Technol. Int. J.* **2022**, *25*, 100986. [CrossRef]
3. Regragui, Y.; Moussa, N. A real-time path planning for reducing vehicles traveling time in cooperative-intelligent transportation systems. *Simul. Model. Pract. Theory* **2023**, *123*, 102710. [CrossRef]
4. Wu, Y.; Wu, L.; Cai, H. A deep learning approach to secure vehicle to road side unit communications in intelligent transportation system. *Comput. Electr. Eng.* **2023**, *105*, 108542. [CrossRef]
5. Zuo, J.; Dong, L.; Yang, F.; Guo, Z.; Wang, T.; Zuo, L. Energy harvesting solutions for railway transportation: A comprehensive review. *Renew. Energy* **2023**, *202*, 56–87. [CrossRef]
6. Yang, Z.; Peng, J.; Wu, L.; Ma, C.; Zou, C.; Wei, N.; Zhang, Y.; Liu, Y.; Andre, M.; Li, D.; et al. Speed-guided intelligent transportation system helps achieve low-carbon and green traffic: Evidence from real-world measurements. *J. Clean. Prod.* **2020**, *268*, 122230. [CrossRef]
7. Chen, Z.; Guo, H.; Yang, J.; Jiao, H.; Feng, Z.; Chen, L.; Gao, T. Fast vehicle detection algorithm in traffic scene based on improved SSD. *Measurement* **2022**, *201*, 111655. [CrossRef]
8. Ribeiro, D.A.; Melgarejo, D.C.; Saadi, M.; Rosa, R.L.; Rodríguez, D.Z. A novel deep deterministic policy gradient model applied to intelligent transportation system security problems in 5G and 6G network scenarios. *Phys. Commun.* **2023**, *56*, 101938. [CrossRef]
9. Sirohi, D.; Kumar, N.; Rana, P.S. Convolutional neural networks for 5G-enabled Intelligent Transportation System: A systematic review. *Comput. Commun.* **2020**, *153*, 459–498. [CrossRef]
10. Lackner, T.; Hermann, J.; Dietrich, F.; Kuhn, C.; Angos, M.; Jooste, J.L.; Palm, D. Measurement and comparison of data rate and time delay of end-devices in licensed sub-6 GHz 5G standalone non-public networks. *Procedia CIRP* **2022**, *107*, 1132–1137. [CrossRef]
11. Wang, Y.; Cao, G.; Pan, L. Multiple-GPU accelerated high-order gas-kinetic scheme for direct numerical simulation of compressible turbulence. *J. Comput. Phys.* **2023**, *476*, 111899. [CrossRef]
12. Sharma, H.; Kumar, N. Deep learning based physical layer security for terrestrial communications in 5G and beyond networks: A survey. *Phys. Commun.* **2023**, *57*, 102002. [CrossRef]
13. Ounoughi, C.; Ben Yahia, S. Data fusion for ITS: A systematic literature review. *Inf. Fusion* **2023**, *89*, 267–291. [CrossRef]
14. Afat, S.; Herrmann, J.; Almansour, H.; Benkert, T.; Weiland, E.; Hölldobler, T.; Nikolaou, K.; Gassenmaier, S. Acquisition time reduction of diffusion-weighted liver imaging using deep learning image reconstruction. *Diagn. Interv. Imaging* **2023**, *104*, 178–184. [CrossRef] [PubMed]
15. Xu, M.; Yoon, S.; Fuentes, A.; Park, D.S. A Comprehensive Survey of Image Augmentation Techniques for Deep Learning. *Pattern Recognit.* **2023**, *137*, 109347. [CrossRef]
16. Zhou, Y.; Ji, A.; Zhang, L.; Xue, X. Sampling-attention deep learning network with transfer learning for large-scale urban point cloud semantic segmentation. *Eng. Appl. Artif. Intell.* **2023**, *117*, 105554. [CrossRef]
17. Yu, C.; Zhang, Z.; Li, H.; Sun, J.; Xu, Z. Meta-learning-based adversarial training for deep 3D face recognition on point clouds. *Pattern Recognit.* **2023**, *134*, 109065. [CrossRef]
18. Kim, C.; Ahn, S.; Chae, K.; Hooker, J.; Rogachev, G. Noise signal identification in time projection chamber data using deep learning model. *Nucl. Instrum. Methods Phys. Res. Sect. A Accel. Spectrometers Detect. Assoc. Equip.* **2023**, *1048*, 168025. [CrossRef]
19. Zhang, X.; Zhai, D.; Li, T.; Zhou, Y.; Lin, Y. Image inpainting based on deep learning: A review. *Inf. Fusion* **2023**, *90*, 74–94. [CrossRef]
20. Mo, W.; Zhang, W.; Wei, H.; Cao, R.; Ke, Y.; Luo, Y. PVDet: Towards pedestrian and vehicle detection on gigapixel-level images. *Eng. Appl. Artif. Intell.* **2023**, *118*, 105705. [CrossRef]
21. Bie, M.; Liu, Y.; Li, G.; Hong, J.; Li, J. Real-time vehicle detection algorithm based on a lightweight You-Only-Look-Once (YOLOv5n-L) approach. *Expert Syst. Appl.* **2023**, *213*, 119108. [CrossRef]
22. Liang, Z.; Huang, Y.; Liu, Z. Efficient graph attentional network for 3D object detection from Frustum-based LiDAR point clouds. *J. Vis. Commun. Image Represent.* **2022**, *89*, 103667. [CrossRef]
23. Tian, Y.; Guan, W.; Li, G.; Mehran, K.; Tian, J.; Xiang, L. A review on foreign object detection for magnetic coupling-based electric vehicle wireless charging. *Green Energy Intell. Transp.* **2022**, *1*, 100007. [CrossRef]
24. Yang, Z.; Pun-Cheng, L.S. Vehicle detection in intelligent transportation systems and its applications under varying environments: A review. *Image Vis. Comput.* **2018**, *69*, 143–154. [CrossRef]
25. Wang, Z.; Ma, Y.; Zhang, Y. Review of pixel-level remote sensing image fusion based on deep learning. *Inf. Fusion* **2023**, *90*, 36–58. [CrossRef]
26. Liu, W.; Anguelov, D.; Erhan, D.; Szegedy, C.; Reed, S.; Fu, C.Y.; Berg, A.C. SSD: Single Shot MultiBox Detector. In *Computer Vision and Pattern Recogniti*; Springer International Publishing: Cham, Switzerland, 2016.
27. Girshick, R.; Donahue, J.; Darrell, T.; Malik, J. Region-Based Convolutional Networks for Accurate Object Detection and Segmentation. *IEEE Trans. Pattern Anal. Mach. Intell.* **2016**, *38*, 142–158. [CrossRef]
28. Jiang, P.; Ergu, D.; Liu, F.; Cai, Y.; Ma, B. A Review of Yolo Algorithm Developments. *Procedia Comput. Sci.* **2022**, *199*, 1066–1073. [CrossRef]

29. Ramachandran, A.; Sangaiah, A.K. A review on object detection in unmanned aerial vehicle surveillance. *Int. J. Cogn. Comput. Eng.* **2021**, *2*, 215–228. [CrossRef]
30. Kim, J.A.; Sung, J.Y.; Park, S.H. Comparison of Faster-RCNN, YOLO, and SSD for Real-Time Vehicle Type Recognition. In Proceedings of the 2020 IEEE International Conference on Consumer Electronics—Asia (ICCE-Asia), Seoul, Republic of Korea, 1–3 November 2020.
31. Qiu, Q.; Lau, D. Real-time detection of cracks in tiled sidewalks using YOLO-based method applied to unmanned aerial vehicle (UAV) images. *Autom. Constr.* **2023**, *147*, 104745. [CrossRef]
32. Dang, F.; Chen, D.; Lu, Y.; Li, Z. YOLOWeeds: A novel benchmark of YOLO object detectors for multi-class weed detection in cotton production systems. *Comput. Electron. Agric.* **2023**, *205*, 107655. [CrossRef]
33. Li, M.; Zhang, Z.; Lei, L.; Wang, X.; Guo, X. Agricultural Greenhouses Detection in High-Resolution Satellite Images Based on Convolutional Neural Networks: Comparison of Faster R-CNN, YOLO v3 and SSD. *Sensors* **2020**, *20*, 4938. [CrossRef] [PubMed]
34. Azimjonov, J.; Özmen, A. A real-time vehicle detection and a novel vehicle tracking systems for estimating and monitoring traffic flow on highways. *Adv. Eng. Inform.* **2021**, *50*, 101393. [CrossRef]
35. Han, X.; Chang, J.; Wang, K. Real-time object detection based on YOLO-v2 for tiny vehicle object. *Procedia Comput. Sci.* **2021**, *183*, 61–72. [CrossRef]
36. Tao, C.; He, H.; Xu, F.; Cao, J. Stereo priori RCNN based car detection on point level for autonomous driving. *Knowl. -Based Syst.* **2021**, *229*, 107346. [CrossRef]
37. Zhang, Q.; Hu, X.; Yue, Y.; Gu, Y.; Sun, Y. Multi-object detection at night for traffic investigations based on improved SSD framework. *Heliyon* **2022**, *8*, e11570. [CrossRef]
38. Shawon, A. Road Traffic Video Monitoring. 2020. Available online: https://www.kaggle.com/datasets/shawon10/road-traffic-video-monitoring?select=traffic_detection.mp4 (accessed on 1 January 2021).
39. Shah, A. Highway Traffic Videos Dataset. 2020. Available online: https://www.kaggle.com/datasets/aryashah2k/highway-traffic-videos-dataset (accessed on 1 March 2020).
40. Saha, S. A Comprehensive Guide to Convolutional Neural Networks—The ELI5 Way. 2018. Available online: https://towardsdatascience.com/a-comprehensive-guide-to-convolutional-neural-networks-the-eli5-way-3bd2b1164a53 (accessed on 15 December 2018).
41. Ding, J.; Li, X.; Kang, X.; Gudivada, V.N. Augmentation and evaluation of training data for deep learning. In Proceedings of the 2017 IEEE International Conference on Big Data (Big Data), Boston, MA, USA, 11–14 December 2017.
42. Phuong, T.M.; Diep, N.N. Speeding Up Convolutional Object Detection for Traffic Surveillance Videos. In Proceedings of the 2018 10th International Conference on Knowledge and Systems Engineering (KSE), Ho Chi Minh City, Vietnam, 1–3 November 2018.
43. Tian, Y.; Su, D.; Lauria, S.; Liu, X. Recent advances on loss functions in deep learning for computer vision. *Neurocomputing* **2022**, *497*, 129–158. [CrossRef]
44. Girshick, R.; Donahue, J.; Darrell, T.; Malik, J. Rich feature hierarchies for accurate object detection and semantic segmentation. In Proceedings of the IEEE Conference on Computer Vision and Pattern Recognition, Columbus, OH, USA, 23–28 June 2014.
45. Redmon, J.; Divvala, S.; Girshick, R.; Farhadi, A. You Only Look Once: Unified, Real-Time Object Detection. In Proceedings of the 2016 IEEE Conference on Computer Vision and Pattern Recognition (CVPR), Las Vegas, NV, USA, 27–30 June 2016.
46. Redmon, J.; Farhadi, A. YOLO9000: Better, Faster, Stronger. In Proceedings of the 2017 IEEE Conference on Computer Vision and Pattern Recognition (CVPR), Honolulu, HI, USA, 21–26 July 2017.
47. Redmon, J.; Farhadi, A. Yolov3: An incremental improvement. *arXiv* **2018**, arXiv:1804.02767.
48. Bochkovskiy, A.; Wang, C.-Y.; Liao, H.-Y.M. Yolov4: Optimal speed and accuracy of object detection. *arXiv* **2020**, arXiv:2004.10934.
49. Jocher, G. Yolov5. Code Repository. 2020. Available online: https://github.com/ultralytics/yolov5 (accessed on 1 July 2020).
50. Li, C.; Li, L.; Jiang, H.; Weng, K.; Geng, Y.; Li, L.; Ke, Z.; Li, Q.; Cheng, M.; Nie, W.; et al. YOLOv6: A single-stage object detection framework for industrial applications. *arXiv* **2022**, arXiv:2209.02976.
51. Wang, C.-Y.; Bochkovskiy, A.; Liao, H.-Y.M. YOLOv7: Trainable bag-of-freebies sets new state-of-the-art for real-time object detectors. *arXiv* **2022**, arXiv:2207.02696.
52. Girshick, R. Fast r-cnn. In Proceedings of the IEEE International Conference on Computer Vision, Santiago, Chile, 7–13 December 2015.
53. Chen, X.; Gupta, A. An implementation of faster rcnn with study for region sampling. *arXiv* **2017**, arXiv:1702.02138.
54. Powers, D.M. Evaluation: From precision, Recall and F-measure to ROC, informedness, markedness and correlation. *arXiv* **2020**, arXiv:2010.16061.
55. Vostrikov, A.; Chernyshev, S. Training sample generation software. In *Intelligent Decision Technologies 2019, Proceedings of the 11th KES International Conference on Intelligent Decision Technologies (KES-IDT 2019), St. Julians, Malta, 17–19 June 2019*; Springer: Berlin/Heidelberg, Germany, 2019; Volume 2.
56. Lin, T.Y.; Maire, M.; Belongie, S.; Hays, J.; Perona, P.; Ramanan, D.; Dollár, P.; Zitnick, C.L. Microsoft coco: Common objects in context. In *Computer Vision–ECCV 2014, Proceedings of the 13th European Conference, Zurich, Switzerland, 6–12 September 2014, Part V 13*; Springer: Berlin/Heidelberg, Germany, 2014.
57. Bathija, A.; Sharma, G. Visual object detection and tracking using Yolo and sort. *Int. J. Eng. Res. Technol.* **2019**, *8*, 705–708.
58. Terven, J.; Cordova-Esparza, D. A comprehensive review of YOLO: From YOLOv1 to YOLOv8 and beyond. *arXiv* **2023**, arXiv:2304.00501.

59. Song, H.; Liang, H.; Li, H.; Dai, Z.; Yun, X. Vision-based vehicle detection and counting system using deep learning in highway scenes. *Eur. Transp. Res. Rev.* **2019**, *11*, 51. [CrossRef]
60. Neupane, B.; Horanont, T.; Aryal, J. Real-Time Vehicle Classification and Tracking Using a Transfer Learning-Improved Deep Learning Network. *Sensors* **2022**, *22*, 3813. [CrossRef] [PubMed]